plications in Science, Medicine, and Industry (Inouye, M., & Sarma, R., Eds.) pp 95-110, Academic Press, New York.
Lory, S., & Collier, R. J. (1980) *Proc. Natl. Acad. Sci. U.S.A. 77*, 267-271.
Lory, S., Carroll, S. F., Bernard, P. D., & Collier, R. J. (1980) *J. Biol. Chem. 255*, 12011-12015.
Marnell, M. H., Shia, S. P., Stookey, M., & Draper, R. K. (1984) *Infect. Immun. 44*, 145-150.
McKeever, B., & Sarma, R. (1982) *J. Biol. Chem. 257*, 6923-6925.
Misler, S. (1984) *Biophys. J. 45*, 107-109.
Montecucco, C., Schiavo, G., & Tomasi, M. (1985) *Biochem. J. 231*, 123-128.
Moskaug, J. O., Sletten, K., Sandvig, K., & Olsnes, S. (1989) *J. Biol. Chem. 264*, 15709-15713.
Murphy, J. R. (1985) *Curr. Top. Microbiol. Immunol. 118*, 235-251.
Olsnes, S., Moskaug, J. O., Stenmark, H., & Sandvig, K. (1988) *Trends Biochem. Sci. 13*, 348-351.
Papini, E., Colonna, R., Cusinato, F., Montecucco, C., Tomasi, M., & Rappuoli, R. (1987a) *Eur. J. Biochem. 169*, 629-635.
Papini, E., Schiavo, G., Tomasi, M., Colombatti, M., Rappuoli, R., & Montecucco, C. (1987b) *Eur. J. Biochem. 169*, 637-644.
Papini, E., Sandona, D., Rappuoli, R., & Montecucco, C. (1988) *EMBO J. 7*, 3353-3359.
Papini, E., Schiavo, G., Rappuoli, R., & Montecucco, C. (1990) *Toxicon 28*, 631-635.
Pappenheimer, A. M., Jr. (1977) *Annu. Rev. Biochem. 46*, 69-94.
Ramsay, G., Montgomery, D., Berger, D., & Freire, E. (1989) *Biochemistry 28*, 529-533.
Sandvig, K., & Olsnes, S. (1980) *J. Cell Biol. 87*, 828-832.
Sandvig, K., & Olsnes, S. (1981) *J. Biol. Chem. 256*, 9068-9076.
Sandvig, K., & Olsnes, S. (1988) *J. Biol. Chem. 263*, 12352-12359.
Sandvig, K., Tonnessen, T. I., Sand, O., & Olsnes, S. (1988) *J. Biol. Chem. 261*, 11639-11644.
Shiver, J. W., & Donovan, J. J. (1987) *Biochim. Biophys. Acta 903*, 48-55.
Stenmark, H., McGill, S., Olsnes, S., & Sandvig, K. (1989) *EMBO J. 8*, 2849-2853.
Ward, W. H. J. (1987) *Trends Biochem. Sci. 12*, 182.
Wharton, S. A., Martin, S. R., Ruigrok, R. W. H., Skehel, J. J., & Wiley, D. C. (1988) *J. Gen. Virol. 69*, 1847-1857.
Williams, D. P., Snider, C. E., Strom, T. B., & Murphy, J. R. (1990) *J. Biol. Chem. 265*, 11885-11889.
Zalman, L. S., & Wisnieski, B. J. (1984) *Proc. Natl. Acad. Sci. U.S.A. 81*, 3341-3345.
Zhao, J.-M., & London, E. (1986) *Proc. Natl. Acad. Sci. U.S.A. 83*, 2002-2006.
Zhao, J.-M., & London, E. (1988a) *J. Biol. Chem. 263*, 15369-15377.
Zhao, J.-M., & London, E. (1988b) *Biochemistry 27*, 3398-3403.

Molecular Dynamics Simulations of the Unfolding of an α-Helical Analogue of Ribonuclease A S-Peptide in Water†

Julian Tirado-Rives* and William L. Jorgensen*
Department of Chemistry, Yale University, New Haven, Connecticut 06511
Received September 14, 1990; Revised Manuscript Received December 7, 1990

ABSTRACT: Molecular dynamics simulations of the S-peptide analogue AETAAAKFLREHMDS have been conducted in aqueous solution for 300 ps at 278 K and for 500 ps in two different runs at 358 K. The results show agreement with experimental observations in that at low temperature, 5 °C, the helix is stable, while unfolding is observed at 85 °C. In the low-temperature simulation a solvent-separated ion pair was formed between Glu-2 and Arg-10, and the side chain of His-12 reoriented toward the C-terminal end of the α-helix. Detailed analyses of the unfolding pathways at high temperature have also revealed that the formation or disappearance of main-chain helical hydrogen bonds occurs frequently through an $\alpha \rightleftharpoons 3_{10} \rightleftharpoons$ no hydrogen bond sequence.

It is well known that proteins display a widely varied range of distinct three-dimensional structures and topologies based on a very limited "alphabet" of only twenty L-amino acids (Richardson, 1981), albeit in am almost infinite number of possible combinations. Given that the spatial arrangement of the atoms of a given protein determines most of its properties, including catalytic power and specificity, correlating the residue sequence to the three-dimensional structure has been a long sought goal. In spite of the apparent enormity of the problem, a large stimulus was provided by the classical experiments of Anfinsen on the unfolding and refolding of ribonuclease A in vitro (White & Anfinsen, 1959). These experiments showed that the amino acid sequence of ribonuclease A contains enough information to provide folding into the "correct" (i.e., native) conformation. This phenomenon has been observed subsequently for other small single-domain proteins (Baldwin, 1989). The many attempts to formulate models that explain how a given amino acid sequence folds into the specific three-dimensional structure of the corresponding protein have given rise to the so-called "protein-folding" problem (King, 1989).

Previous investigations on the folding pathways of proteins have lead to the development of two general classes of models, kinetic and structural. The kinetic models have been derived

†Supported by NIH Grant GM 32136.

0006-2960/91/0430-3864$02.50/0

mostly from rate and thermodynamic studies on the folding and unfolding of proteins and are as such typically expressed in terms of the number of intermediates detected, their stabilities, and their kinetic behavior toward folding, rather than in terms of structural or conformational details (Kim & Baldwin, 1982). Structural models, on the other hand, have been developed from the examination of known structures of folded proteins. Some recent studies have attempted to bridge between the two classes of models through the characterization of large fragments of staphylococcal nuclease incapable of complete folding (Shortle & Meeker, 1989) and through folding studies of some of its mutant forms (Shortle & Meeker, 1986). It is only recently that some experimental protocols have evolved to the point where they can provide structural details on transient intermediates. In particular, hydrogen-exchange labeling experiments have been utilized to assess via 2-D NMR the degrees of protection of different sites at intermediate times during refolding experiments on ribonuclease A (Udgaonkar & Baldwin, 1988), cytochrome *c* (Roder et al., 1988), α-lactalbumin (Baum et al., 1989), and barnase (Bycroft et al., 1990).

Currently, the most accepted structural hypotheses of protein folding are represented by the "molten globule" (Ptitsyn, 1987), "framework" (Anfinsen, 1972; Richmond & Richards, 1978), and "jigsaw puzzle" (Harrison & Durbin, 1985) models. The latter corresponds very closely to the kinetic diffusion–collision model (Karplus & Weaver, 1979). Despite their conceptual differences these schemes all involve the early formation of local regions of secondary structure, particularly α-helices, that subsequently associate or rearrange to form the complete three-dimensional protein (Montelione & Scheraga, 1989). The understanding of the pathways of formation for these structural elements and of their stability should then provide valuable insights into the folding problem.

The experimental study of α-helices in small isolated peptides has been hindered by their intrinsic instability in aqueous solution. In fact, after many studies of natural and synthetic peptides [see, for instance, Panijpan and Gratzer (1974); Wagman et al. (1980); Hammes and Schullery (1968)] and particularly after the development of the stability (s) and nucleation (σ) constants for all the amino acids through host–guest copolymers (Scheraga, 1978), it was believed that α-helices formed by small peptides (≤20 residues) were not stable in solution. The first exception found to this generalization was the S-peptide, isolated by subtilisin cleavage of the first 19–20 residues of ribonuclease A. When separated from the rest of the protein, this peptide is ca. 30% helical at 0 °C (Klee, 1968). In a very extensive series of CD studies of S-peptide, C-peptide (obtained from the cyanogen bromide cleavage of ribonuclease A), and many synthetic analogues, Baldwin and co-workers have proposed explanations for the stability of these small helices in terms of specific interactions such as salt bridges (Bierzynski et al., 1982; Kim et al., 1982) and charge–helix dipole interactions (Shoemaker et al., 1985, 1987; Fairman et al., 1989). Other stable helices in small peptides are Pα5, corresponding to residues 47–58 in the C terminus of bovine pancreatic trypsin inhibitor, which is 8–23% helical at 0 °C (Goodman & Kim, 1989), and some de novo designed peptides based on polyalanine with regular Lys and Glu insertions, which have been determined to contain as much as 80% helix at 0 °C (Marqusee & Baldwin, 1987; Marqusee et al., 1989).

The theoretical study of α-helices, particularly with molecular dynamics simulations, should be valuable in providing insights not only on the factors affecting stability but also on the pathways followed during folding and unfolding. To date there have been few papers published on this subject, and most of these utilize greatly simplified representations of the solute and the solvent to reduce the computational demands. A common technique represents each amino acid residue as a single interaction site and utilizes approximate corrections for the effect of the solvent. Some reported applications include simulations of the folding of BPTI from extended structures by minimization–normal mode thermalization (Levitt, 1976; Warshel & Levitt, 1975), the simulation of the folding of rigid preformed helices in carp myogen (Warshel & Levitt, 1976) by the same method, and a stochastic dynamics simulation of the unfolding of a helical peptide composed of 15 valine residues (Brooks et al., 1988). Another technique features simplified interaction models for the residues as well but additionally imposes discretization of the available space by constraining the interaction sites to occupy positions given by the vertices of different regular lattices [see, for instance, Krigbaum and Lin (1982); Taketoni et al. (1988); Chan and Dill (1989); Sikorski and Skolnick (1990)].

In this setting, the present simulations were undertaken to study the unfolding of a small α-helical peptide by using full atomic representations for both the peptide and the solvent water via molecular dynamics. The direction of unfolding was chosen for study in preference to folding in order to take advantage of the fact that the structure of folded peptides is much better defined than that of their unfolded counterparts. In addition, following the unfolding process provides a convenient way to circumvent the potential difficulties caused by the likely existence of multiple minima in the folding pathway. A 15-residue analogue of S-peptide (Mitchinson & Baldwin, 1986) was initially chosen among the many sequence variants of the S- and C-peptides as a starting point. The sequence of this peptide is compared to the initial part of the native S-peptide as follows:

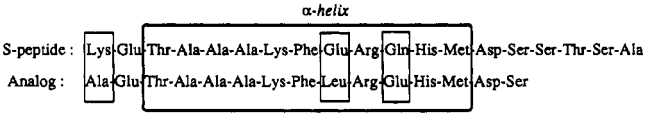

This analogue has several advantages for the theoretical study of unfolding. Experimental data are available for comparison and reveal that the peptide has a considerable population of the helical form in water at low temperature (≥45% at 276 K) and a convenient thermal stability range; the ellipticity curves of such analogues are essentially flat for $T \geq 333$ K. MD simulations can therefore be conducted under realistic conditions at temperatures that would favor either the folding or unfolding of the helix. The peptide also has no net charge at neutral pH, so counterions are not needed to maintain electrical neutrality. In addition, the present study could be used as the starting point for a series of simulations that explores the effects of residue substitutions on the folding process. Other studies could utilize statistical perturbation theory (Jorgensen & Ravimohan, 1985) to evaluate the effects of residue substitutions on the free energies of folding or unfolding; and importantly, the amino acid sequence of the chosen peptide is very similar to the corresponding segment of ribonuclease A, so a good starting point may be obtained from an available crystal structure with only minor modifications.

Experimental Procedures

Computational Methods. Except where noted all simulations were conducted on Sun-4 computers using the AMBER

3.0 software (Singh et al., 1986) with minor local modifications to improve its use of the UNIX environment. The OPLS nonbonded parameters (Jorgensen & Tirado-Rives, 1988), including the all-atom parameters recently developed for aromatic rings (Jorgensen & Severance, 1990), were used for the peptide atoms in conjunction with the TIP3P model for water (Jorgensen et al., 1983). As specified in the OPLS model, the dielectric constant was fixed at 1.0, and the scaling factors for the 1,4-nonbonded interactions were 8.0 for the Lennard-Jones and 2.0 for the electrostatic interactions. The energetics for angle bending and torsional motion were described with the AMBER force field (Weiner et al., 1984). During the simulations all bond lengths and the H–H distances in water were fixed at their equilibrium values by using the SHAKE algorithm (van Gunsteren & Berendsen, 1977) with a tolerance of 0.0004 Å, which allowed a time step of 2 fs. A nonbonded pair list was used to accelerate the calculations and was updated every 10 steps. This list was generated by using a 9-Å residue-based cutoff to avoid splitting dipoles. All calculations utilized periodic boundary conditions to avoid edge effects. The pressure was fixed at 1 bar (0.987 atm) in all NPT dynamics simulations.

The initial coordinates were obtained from the X-ray structure of ribonuclease S (Fletterick & Wyckoff, 1975) as deposited in the Brookhaven Protein Data Bank, entry 1RNS (Bernstein et al., 1977). The first 15 residues were extracted, and the appropriate residue substitutions (1 Lys/Ala, 9 Glu/Leu, 11 Gln/Glu) were made by using the SYBYL software from Tripos Associates on a Silicon Graphics Iris-4D/25G computer. The polar and aromatic hydrogen atoms were then added, and local minimization was used to correct the conformation of the modified residues. The resulting peptide molecule was then centered in a rectangular box of water obtained by periodic translations in the x, y, and z directions of a cube of TIP3P water previously equilibrated via Monte Carlo calculations. Any water molecule with oxygen-to-solute or hydrogen-to-solute distances less than 2.0 or 0.5 Å, respectively, or farther than 7.0 Å from the closest peptide atom in any one Cartesian direction was then deleted to give an initial system containing the solute plus 892 water molecules (2827 total atoms) in a rectangular box of dimensions 40.8 × 27.3 × 25.3 Å.

The preliminary preparation of the system, geared toward the relief of bad solute–solvent interactions, was for the most part conducted by keeping the peptide molecule fixed in a "belly" (i.e., by setting the forces acting on the atoms to zero). The initial step consisted of 100 cycles of steepest descent energy minimization at constant volume followed by a 3-ps constant-volume molecular dynamics run, during which the temperature was gradually increased from an initial 100 to 278 K. The resulting structure was equilibrated at 278 K through an additional 5 ps of NVT-MD. The peptide was then allowed to move along with the solvent in a 1-ps NVT-MD run at 278 K in which the initial atomic velocities were assigned from a Maxwellian distribution corresponding to a temperature of 150 K. Two different NPT-MD calculations were started from this configuration in order to favor either folding or unfolding behavior, a "cold" one (abbreviated C) at 278 K in which the initial atomic velocities were assigned from a Maxwellian distribution corresponding to a temperature of 150 K and a "hot" one (abbreviated H1) at 358 K in which the initial atomic velocities were assigned from a Maxwellian distribution corresponding to a temperature of 210 K. A second "hot" (abbreviated H2) simulation at 358 K was subsequently started by doing an unconstrained minimization in vacuo of the initial peptide with a distance-dependent dielectric constant ($\epsilon = 8R$) and following the same procedure described above.

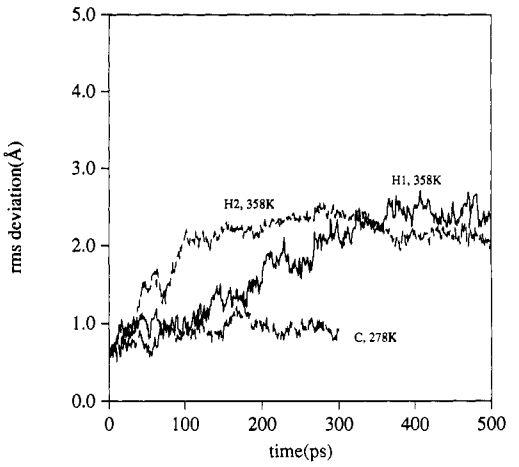

FIGURE 1: Plots of the RMS deviations of the main-chain heavy atoms for the three simulations.

The values of the potential energy, RMS deviation from the initial structure, and volume were monitored continuously in order to assess the evolution of the system. Total simulation times were 300 ps for the cold and 500 ps for both hot simulations. During these times the coordinates, velocities, and energies were saved every 50 time steps (0.1 ps) for further analysis.

RESULTS

The RMS deviations from the modified crystal structure for the main-chain atoms (N, C^{α}, C, and O) of residues 3–13 in the three simulations are plotted in Figure 1 as a function of simulation time. The deviations of the instantaneous structures at the end of each simulation are 0.930 Å after 300 ps for run C at 278 K, and 2.300 and 2.086 Å after 500 ps for runs H1 and H2 at 358 K, respectively. Although the absolute numbers as given are not indicative of the quality of the structures, they reflect the overall structural change undergone by the peptide during the simulations. As expected from the additional kinetic energy available, the simulations at the higher temperature display considerably large deviations from the initial structure than the lower temperature run.

The instantaneous structure after 300 ps of the 278 K simulation still contains the helix from residues 3 to 13 present in the crystal structures of both ribonuclease S (Fletterick & Wyckoff, 1975) and ribonuclease A (Wlodawer et al., 1988). Six of the seven main-chain hydrogen bonds are conserved, the only exception being the hydrogen bond between Ala-6 and Arg-10, which is replaced by 3_{10}-type hydrogen bond between Lys-7 and Arg-10. Throughout the present study, a hydrogen bond was considered formed if the hydrogen to acceptor atom distance was less than 2.5 Å and the donor–hydrogen–acceptor angle was between 120° and 180°. The movements of the main chain in the course of the cold simulation can be followed in the stereodiagrams presented in Figure 2. The first two residues are floppier than the helical portion of the peptide. Also, both α- and 3_{10}-type hydrogen bonds are well populated as the simulation progresses. The populations of the different main-chain hydrogen bonds during the entire length of this simulation are given in Table I and show a very high degree of conservation (≥90%) for the hydrogen bonds from Ala-4 to Phe-8, Ala-5 to Leu-9, and Phe-8 to His-12. The termini of the helix display considerable fraying as reflected in the lower populations of the Thr-3 to Lys-7 and

Table I: Populations of Main-Chain Hydrogen Bonds for the Different Simulations[a]

acceptor (O)	donor (N-H)	helix type	simulation[b] C (278)	H1 (358)	H2 (358)
Thr-3	Lys-7	α	56.6	44.3	25.5
Ala-4	Lys-7	3_{10}	26.2	42.5	28.4
Ala-4	Phe-8	α	97.3	52.5	42.7
Ala-5	Phe-8	3_{10}	18.5	37.2	11.3
Ala-5	Leu-9	α	93.3	74.1	34.9
Ala-6	Leu-9	3_{10}	4.9	16.4	12.0
Ala-6	Arg-10	α	48.0	4.1	3.1
Lys-7	Arg-10	3_{10}	59.6	31.6	20.8
Lys-7	Glu-11	α	49.3	5.4	6.9
Phe-8	Glu-11	3_{10}	61.4	15.5	1.5
Phe-8	His-12	α	90.1	14.1	6.6
Leu-9	His-12	3_{10}	0.0	1.9	0.0
Leu-9	Met-13	α	42.5	16.5	0.0
Arg-10	Met-13	3_{10}	8.3	0.1	0.0

[a] Values are given in percent. [b] Numbers in parentheses indicate the temperature (K).

Leu-9 to Met-13 hydrogen bonds, 56.6 and 42.5 %, respectively. The two remaining hydrogen bonds, Ala-6 to Arg-10 and Lys-7 to Glu-11, show conservations comparable to the termini, but there is compensation from a higher population of the corresponding 3_{10}-type hydrogen bonds from Lys-7 to Arg-10 and from Phe-8 to Glu-11, which maintain the integrity of the helix. In fact, the N-H groups of Arg-10 and Glu-11 spend larger amounts of time engaged in hydrogen bonds of the 3_{10}- rather than the α-type. Table II presents a very coarse-grained history for the main-chain hydrogen bonds during the simulations. In this table, the hydrogen bond from each donor N-H (in horizontal rows) is represented in columns corresponding to consecutive 25-ps segments of the simulation by an α or a 3, depending on whether the α- or the 3_{10}-helical type had more than a 50% occurrence during that period. Overall, the helix was preserved quite well during the course of the entire simulation at 278 K.

The H1 and H2 simulations at 358 K provided significantly more movement as reflected in the representations of the main-chain atoms at different times in Figures 3 and 4. The helical portions of the peptide are noticeably distorted from early in the simulations. In run H1, which started from the same structure as the low-temperature simulation, the three hydrogen bonds closest to the C terminus are broken within 155 ps, and the fourth one disappears before 200 ps (Table II). The three N-terminal hydrogen bonds remain largely intact for the rest of the simulation in either the α- or the 3_{10}-helical form. In the period from 230 to 500 ps, after loss of the C-terminal hydrogen bonds is complete, the populations of either type of helical hydrogen bonds formed by the N-H groups of Lys-7, Phe-8, and Leu-9 are 81%, 65%, and 96%, respectively. It is also seen from the stereoplots (Figure 3) that during run H1 the peptide unravels at the C-terminal end, then it folds back on itself with a bend near residue 11 and extension of residues 12–15 toward the N terminus.

In the other 358 K run (H2) the three C-terminal hydrogen bonds are broken within 40 ps, and all the helical hydrogen bonds have vanished by 155 ps (Table II and Figure 4). Remarkably, the first three N-terminal hydrogen bonds reformed between 360 and 380 ps and stayed, again in either the α- or the 3_{10}-form, for the remainder of the simulation in a manner similar to that of simulation H1. In the period from 360 to 500 ps, the populations of either type of helical hydrogen bonds formed by the N-H groups of Lys-7, Phe-8, and Leu-9 are 78%, 79%, and 69%, respectively. However, in this trajectory, the peptide does not fold back on itself but progresses to a more elongated structure (Figure 4).

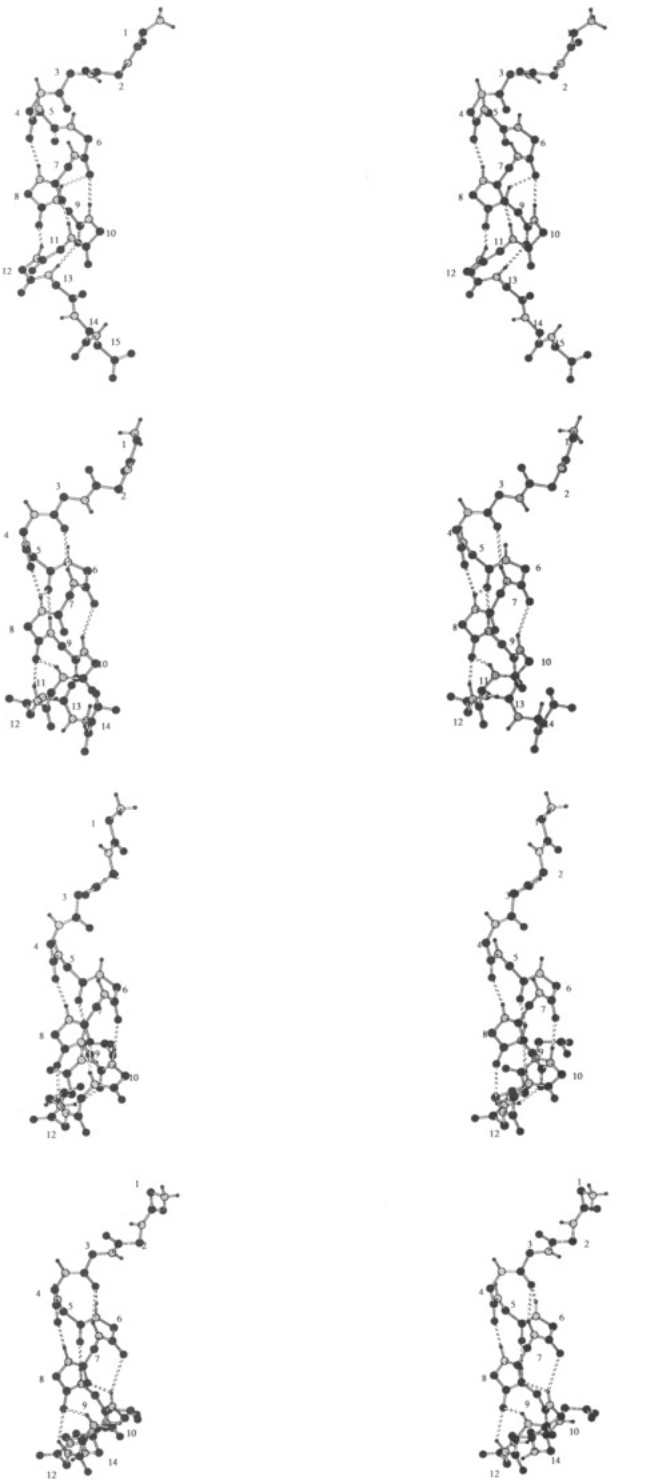

FIGURE 2: Main-chain atoms at 0, 84, 180, and 300 ps from top to bottom during simulation C at 278 K.

The general result observed in both simulations at 358 K is the unfolding of the helical portion of the peptide. Of all the main-chain hydrogen bonds, the three nearest the N terminus of the helix are the only ones remaining at the end of 500 ps in these simulations. The first two among these also show a relatively high content of 3_{10}-type helix, 37% and 49% in the last 270 ps of simulation H1 and 45% and 24% in the last 140 ps of simulation H2.

Discussion

The most striking movements observed for the side chains of the helical portion of the peptide during the course of sim-

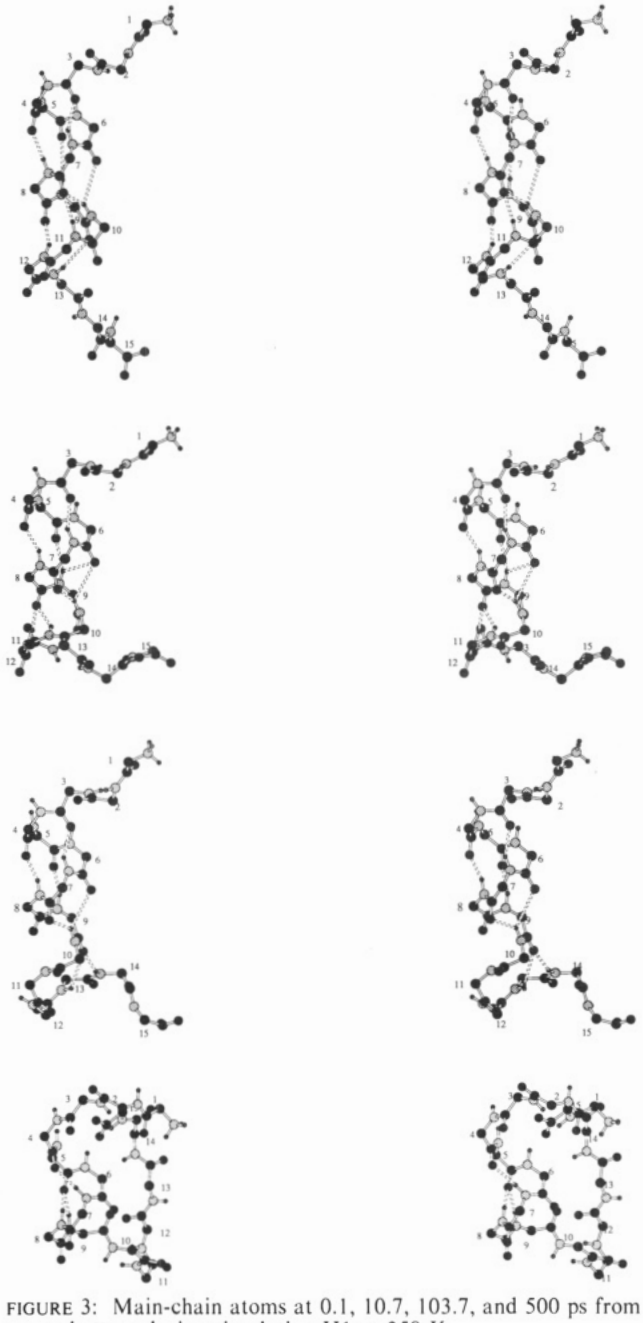

FIGURE 3: Main-chain atoms at 0.1, 10.7, 103.7, and 500 ps from top to bottom during simulation H1 at 358 K.

FIGURE 4: Main-chain atoms at 0.1, 101, 300, and 500 ps from top to bottom during simulation H2 at 358 K.

ulation C at 278 K are a drifting apart of the negatively charged carboxylate side chain of Glu-2 and the positively charged guanidinium part of Arg-10 to form a solvent-separated ion pair, instead of the starting contact ion pair, and the turn of the side chain of His-12 toward the C-terminal end of the α-helix. These displacements can be appreciated clearly in the comparison of the instantaneous structures at 1.0 and 110.0 ps presented in Figure 5. The solvent-separated ion pair involves three different water molecules at different times from its initial formation at 57 ps until the end of the simulation at 300 ps, although from 57 to 70 ps two of them are simultaneously bound as seen in the bottom structure of Figure 5. The water-bridging association is also lost when the charged groups drift farther apart at 148 ps just to be formed again at 226 ps.

The movement of the histidine side chain, complete at 70 ps, locates the positive charge on the imidazolium unit in a more favorable position to take advantage of the charge–helix dipole-stabilizing interaction suggested by Baldwin (Shoemaker et al., 1985, 1987; Fairman et al., 1989). This motion is also observed, albeit only transiently due to the unfolding of the helix, in the initial portion of simulations H1 and H2 at 358 K, where it is completed at 13 and 17 ps, respectively. A similar orientation of a His side chain at the C terminus of an α-helix has been observed in the protein barnase (Šali et al., 1988), where it has been used to explain the anomalously high pK_a for the histidine.

The higher stability of the three hydrogen bonds near the N terminus of the helix observed in both high-temperature simulations is consistent with the higher helical propensity of the residues involved, most notably the Ala-4, Ala-5, and Ala-6 triad. Figure 6 shows the results of applying two different methods of secondary structure prediction, the Chou–Fasman approach (Chou & Fasman, 1978) and the Scheraga modification of the Zimm–Bragg method (Vasquez et al., 1987), to the S-peptide analogue in this study. Both treatments are

Table II: Helical Type for the Main-Chain Hydrogen Bonds during the Simulations

donor	25	50	75	100	125	150	175	200	225	250	275	300	325	350	375	400	425	450	475	500
Simulation C, 300 ps at 278 K																				
13		3					α	α	α	α	α									
12	α	α	α	α	α	α	α	α	α	α	α	α								
11	α	α	α	3	3	α	3	3	3	3	3	3								
10	3	3	α	α	3	α	α	α	α	α	3	3								
9	α	α	α	α	α	α	α	α	α	α	α	α								
8	α	α	α	α	α	α	α	α	α	α	α	α								
7	α	α	α	α	3	3			α	α	α	α								
Simulation H1, 500 ps at 358 K																				
13		α	α	α		α														
12	α	α	α																	
11	3	3	3	3																
10	3	3	3	3	3	3	3	3												
9	α	α	α	α		α	3	α	α	3	α	α	α	α	α	α	α	α	α	α
8	α	α	α	α	α	α	α	α	α	3	3	3		3				3		3
7	α		3					3		α		3	α	3	α	α	α		α	
Simulation H2, 500 ps at 358 K																				
13																				
12	α																			
11	α																			
10	3	3	3	3																
9	α	α	α		α											α		α	α	α
8	α	α	α	α	α	α										α	3	α	α	α
7	α	3	3	3	3	α										α		α	3	3

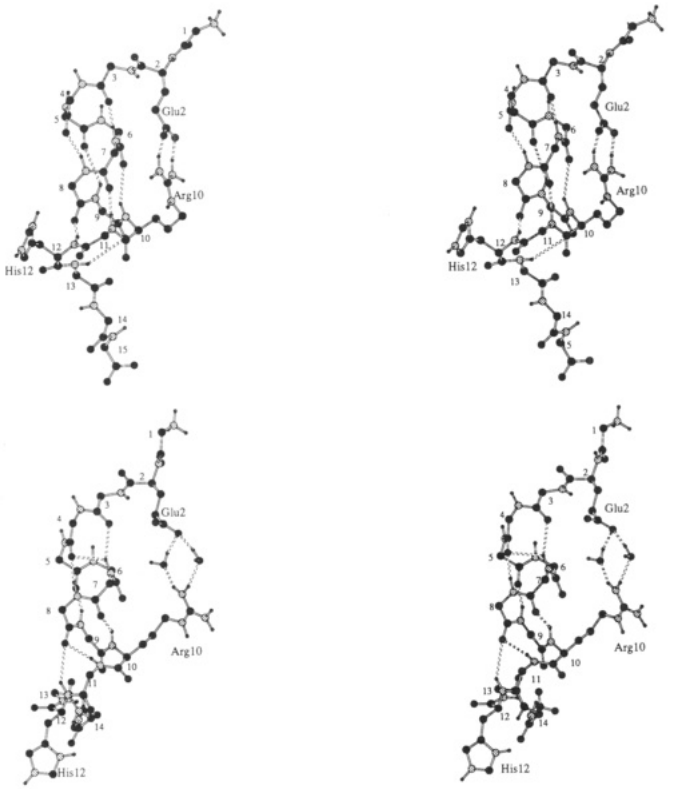

FIGURE 5: Comparison of structures at 1.0 (top) and 110.0 ps (bottom) for simulation C at 278 K.

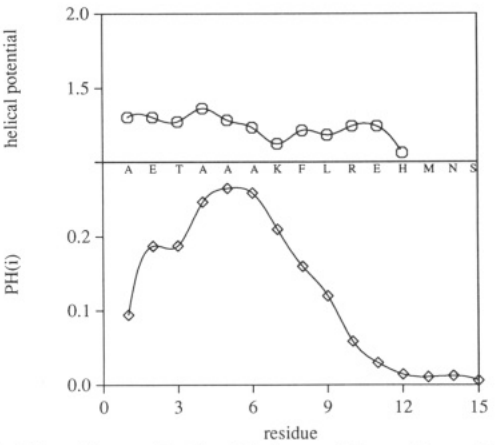

FIGURE 6: Chou–Fasman (top) and Scheraga/Zimm–Bragg (bottom) helical potential predictions.

in agreement in assigning the region containing these residues the greatest helix probability for the chain. The high helix-forming potential of Ala has also been emphasized by Baldwin and co-workers (Marqusee & Baldwin, 1987; Padmanabhan et al., 1990) and is graphically illustrated in Figures 3 and 4.

Other similarities between the high-temperature simulations H1 and H2 are revealed by detailed examination of both the resultant structures and the hydrogen bonding. Most interestingly, a common pattern emerges for the loss or formation of the main-chain hydrogen bonds in the process of unfolding the helix. Of the 13 such events observed in the course of the simulations, 10 occur through the intermediacy of a 3_{10}-type helical hydrogen bond. That is, in the sequence typically observed for a loss, a given N-H donor initially forming an α-helical hydrogen bond between residues i and $i - 4$ shifts from its acceptor carbonyl oxygen to the next carbonyl in the chain to form a new 3_{10}-type hydrogen bond between residues i and $i - 3$ before ultimately breaking away and forming a hydrogen bond to the solvent. It should be noted that due to the intrinsic fluctuations of the backbone dihedral angles in a molecular dynamics simulations at 358 K a single turn of a 3_{10}-helix is conformationally indistinguishable from a reverse turn of type III. An example of this sequence of events, leading to the disappearance of the hydrogen bond between Glu-11 and Lys-7 during simulation H2, is illustrated in Figure 7. The reverse process corresponds to nucleation of an α-helix by first forming a 3_{10} segment as witnessed in the bottom structures of Figure 4.

Additional support for the intermediacy of these conformations comes from crystal structures. In a recent survey of proteins containing water-inserted α-helical regions in the Brookhaven Data Bank, Sundaralingam and Sekharudu (1989) found a number of cases in which reverse turns, mostly of types III and I for segments not containing proline, are

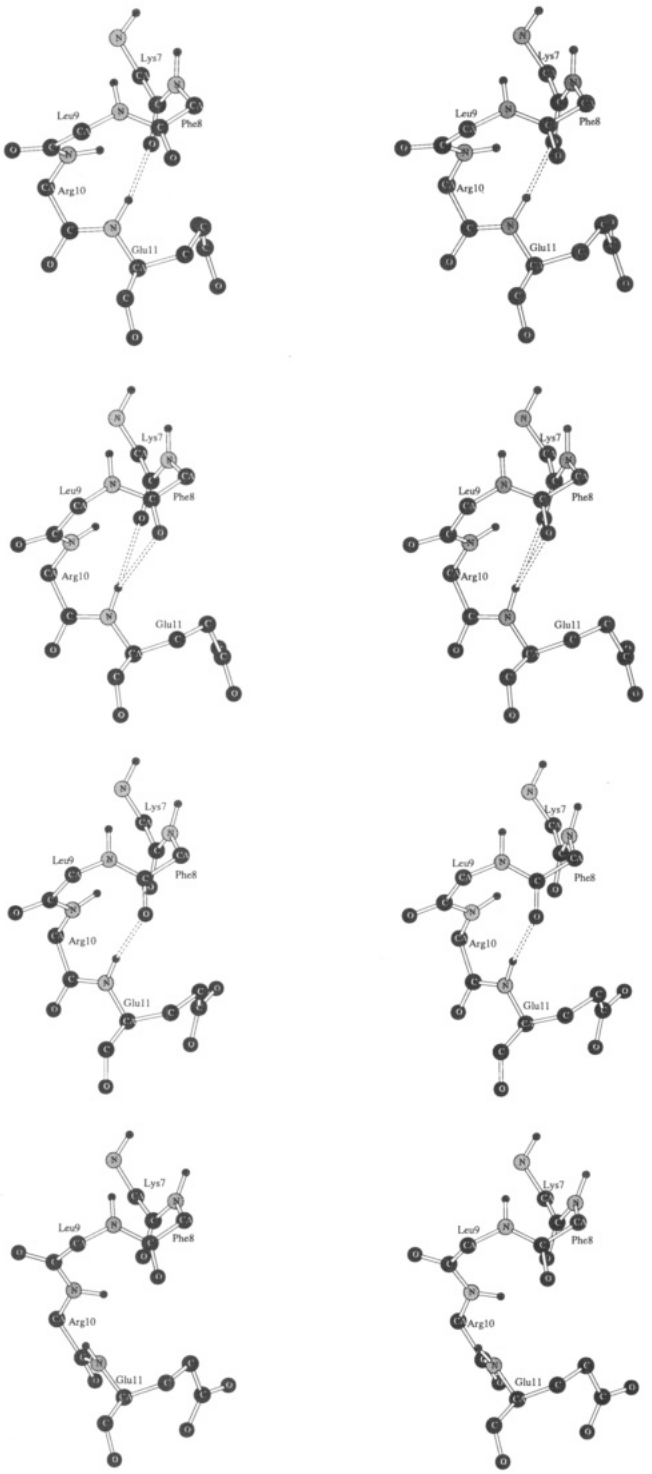

FIGURE 7: Main chain atoms at 35.7, 37.6, 38.9, and 40.7 ps from top to bottom during simulation H2 at 358 K.

formed and proposed them to be intermediates in the folding and unfolding of α-helices. In the course of a 130-ps molecular dynamics simulation of decaalanine at 300 K, Beveridge and co-workers found theoretical support for the insertion of water as a source of destabilization of α-helices (Di Capua et al., 1990) but did not elaborate further on the conformational state of the helix.

In conclusion, the present study demonstrates that molecular dynamics simulations can be utilized to study the unfolding of small helical peptides in water in computationally accessible times by using full atomic representations for both the solute and the solvent. The results show agreement with experimental observations in that at low temperature, 5 °C in the present case, the helix in the S-peptide analogue is quite stable, while unfolding is observed at 85 °C. Furthermore, the unfolding is rapid at 85 °C (ca. 200 ps) and is, therefore, computationally accessible. The detailed analysis of the unfolding pathways for two independent high-temperature simulations has also revealed that very frequently the formation or disappearance of a main-chain helical hydrogen bond occurs through the $\alpha \rightleftharpoons 3_{10} \rightleftharpoons$ no hydrogen bond sequence.

References

Anfinsen, C. B. (1972) *Biochem. J. 128*, 737.

Baldwin, R. L. (1989) *Trends Biochem. Sci. 14*, 291.

Baum, J., Dobson, C. M., Evans, P. A., & Hanley, C. (1989) *Biochemistry 28*, 7.

Bernstein, F. C., Koetzle, T. F., Williams, G. J. B., Meyer, E. F., Jr., Brice, M. D., Rodgers, J. R., Kennard, O., Shimanouchi, T., & Tasumi, M. (1977) *J. Mol. Biol. 112*, 535.

Bierzynski, A., Kim, P. S., & Baldwin, R. L. (1982) *Proc. Natl. Acad. Sci. U.S.A. 79*, 2470.

Brooks, C. L., III, Karplus, M., & Pettitt, B. M. (1988) *Adv. Chem. Phys. 71*, 1.

Bycroft, M., Matouscheck, A., Kellis, J. T., Serrano, L., & Fersht, A. R. (1990) *Nature 346*, 488.

Chan, H. S., & Dill, R. A. (1989) *Macromolecules 22*, 4559.

Chou, P. Y., & Fasman, G. D. (1978) *Adv. Enzymol. Relat. Areas Mol. Biol. 47*, 45.

Di Capua, F. M., Swaminathan, S., & Beveridge, D. L. (1990) *J. Am. Chem. Soc. 112*, 6768.

Fairman, R., Shoemaker, K. R., York, E. J., Stewart, J. M., & Baldwin, R. L. (1989) *Proteins: Struct., Funct., Genet. 5*, 1.

Fletterick, R. J., & Wyckoff, H. W. (1975) *Acta Crystallogr., Sect. A 31*, 698.

Goodman, E. M., & Kim, P. S. (1989) *Biochemistry 28*, 4343.

Hammes, G. G., & Schullery, S. E. (1968) *Biochemistry 7*, 3882.

Harrison, S. C., & Durbin, R. (1985) *Proc. Natl. Acad. Sci. U.S.A. 82*, 4028.

Jorgensen, W. L., & Ravimohan, C. (1985) *J. Chem. Phys. 83*, 3050.

Jorgensen, W. L., & Tirado-Rives, J. (1988) *J. Am. Chem. Soc. 110*, 1657.

Jorgensen, W. L., & Severance, D. L. (1990) *J. Am. Chem. Soc., 112*, 4768.

Jorgensen, W. L., Chandrasekhar, J., Madura, J. D., Impey, R. W., & Klein, M. L. (1983) *J. Chem. Phys. 79*, 926.

Karplus, M., & Weaver, D. (1979) *Biopolymers 18*, 1421.

Kim, P. S., & Baldwin, R. L. (1982) *Annu. Rev. Biochem. 51*, 459.

Kim, P. S., Bierzynski, A., & Baldwin, R. L. (1982) *J. Mol. Biol. 162*, 187.

King, J. (1989) *Chem. Eng. News 67 (15)*, 32.

Klee, W. A. (1968) *Biochemistry 7*, 2731.

Krigbaum, W. R., & Lin, S. F. (1982) *Macromolecules 15*, 1135.

Levitt, M. (1976) *J. Mol. Biol. 104*, 59.

Marqusee, S., & Baldwin, R. L. (1987) *Proc. Natl. Acad. Sci. U.S.A. 84*, 8898.

Marqusee, S., Robbins, V. H., & Baldwin, R. L. (1989) *Proc. Natl. Acad. Sci. U.S.A. 86*, 5286.

Mitchinson, C., & Baldwin, R. L. (1986) *Proteins: Struct., Funct., Genet. 1*, 23.

Montelione, G. T., & Scheraga, H. A. (1989) *Acc. Chem. Res. 22*, 70.

Padmanabhan, S., Marqusee, S., Ridgeway, T., Laue, T. M., & Baldwin, R. L. (1990) *Nature 344*, 268.
Panijpan, B., & Gratzer, W. B. (1974) *Eur. J. Biochem. 45*, 547.
Ptitsyn, O. B. (1987) *J. Protein Chem. 6*, 273.
Richardson, J. S. (1981) *Adv. Prot. Chem. 34*, 167.
Richmond, T. J., & Richards, F. M. (1978) *J. Mol. Biol. 119*, 537.
Roder, H., Elöve, G. A., & Englander, S. W. (1988) *Nature 335*, 700.
Šali, D., Bycroft, M., & Fersht, A. (1988) *Nature 335*, 740.
Scheraga, H. A. (1978) *Pure Appl. Chem. 50*, 315.
Shoemaker, K. R., Kim, P. S., Brems, D. N., Marqusee, S., York, E. J., Chaiken, I. M., Stewart, J. M., & Baldwin, R. L. (1985) *Proc. Natl. Acad. Sci. U.S.A. 82*, 2349.
Shoemaker, K. R., Kim, P. S., York, E. J., Stewart, J. M., & Baldwin, R. L. (1987) *Nature 326*, 563.
Shortle, D. S., & Meeker, A. K. (1986) *Proteins: Struct., Funct., Genet. 1*, 81.
Shortle, D. S., & Meeker, A. K. (1989) *Biochemistry 28*, 936.
Sikorski, A., & Skolnick, J. (1990) *J. Mol. Biol. 212*, 819.
Singh, U. C., Weiner, P. K., Caldwell, J., & Kollman, P. A. (1986) AMBER 3.0, University of California, San Francisco.
Sundaralingam, M., & Sekharudu, Y. C. (1989) *Science 244*, 1331.
Taketoni, H., Kano, F., & Gō, N. (1988) *Biopolymers 27*, 527.
Udgaonkar, J. B., & Baldwin, R. L. (1988) *Nature 335*, 694.
van Gunsteren, W. F., & Berendsen, H. J. C. (1977) *Mol. Phys. 34*, 1311.
Vasquez, M., Pincus, M. R., & Scheraga, H. A. (1987) *Biopolymers 26*, 351.
Wagman, M. E., Dobson, C. M., & Karplus, M. (1980) *FEBS Lett. 119*, 265.
Warshel, A., & Levitt, M. (1975) *Nature 253*, 694.
Warshel, A., & Levitt, M. (1976) *J. Mol. Biol. 106*, 421.
Weiner, S. J., Kollman, P. A., Case, D. A., Singh, U. C., Ghio, C., Alagona, G., Profeta, S., & Weiner, P. J. (1984) *J. Am. Chem. Soc. 106*, 765.
White, F. H., Jr., & Anfinsen, C. B. (1959) *Ann. N. Y. Acad. Sci. 81*, 515.
Wlodawer, A., Svensson, L. A., Sjölin, L., & Gilliland, G. L. (1988) *Biochemistry 27*, 2705.

Reversible Unfolding of Cytochrome *c* upon Interaction with Cardiolipin Bilayers. 1. Evidence from Deuterium NMR Measurements†

Paul J. R. Spooner* and Anthony Watts
Department of Biochemistry, University of Oxford, South Parks Road, Oxford OX1 3QU, U.K.
Received September 11, 1990; Revised Manuscript Received November 29, 1990

ABSTRACT: Deuterium NMR has been used to investigate the structure and dynamic state of cytochrome *c* complexed with bilayers of cardiolipin. Reductive methylation was employed to prepare [N^{ϵ},N^{ϵ}-C^2H_3]lysyl cytochrome *c*, and deuterium exchange provided labeling of backbone sites to give [*amide*-^{2}H]cytochrome *c* or more selective labeling of just histidine residues in [ϵ-^{2}H]histidine cytochrome *c*. Deuterium NMR measurements on [N^{ϵ},N^{ϵ}-C^2H_3]lysyl cytochrome *c* in the solid state showed restricted motions, fairly typical of the behavior of aliphatic side-chain sites in proteins. The [*amide*-^{2}H]cytochrome *c* provided "immobile" amide spectra showing that only the most stable backbone sites remained labeled in this derivative. Relaxation measurements on the aqueous solution of [*amide*-^{2}H]cytochrome *c* yielded a rotational correlation time of 7.9 ns for the protein, equivalent to a hydrodynamic diameter of 4.0 nm, just 0.6 nm greater than its largest crystallographic dimension. Similar measurements on [ϵ-^{2}H]histidine cytochrome *c* in solution showed that all labeled histidine residues were also "immobile" compared with the overall reorientational motion of the protein. The interaction with cardiolipin bilayers appeared to create a high degree of mobility for the side-chain sites of [N^{ϵ},N^{ϵ}-C^2H_3]lysyl cytochrome *c* and perturbed backbone structure to instantaneously release all deuterons in [*amide*-^{2}H]cytochrome *c*. The [ϵ-^{2}H]histidine cytochrome *c* derivative, when complexed with cardiolipin, failed to produce any detectable wide-line ^{2}H NMR spectrum, demonstrating that the overall reorientational motion of bound protein was not isotropic on the NMR time scale, i.e., $\tau_c > 10^{-7}$ s. Additional measurements on the deuterium-exchanged protein–lipid complex, prepared in ^2H_2O, did not reveal any stable amide sites in the protein backbone, providing the lipid remained in its normal liquid-crystalline state. However, stable backbone sites were detected at reduced temperatures where, according to ^{31}P NMR observations, the lipid component was becoming immobilized in the complex. A strong binding of protein with liquid-crystalline bilayers of cardiolipin disorders the lysine sites of interaction on the surface of the protein and appears to cause an extensive derangment of secondary structure, such that no stable α-helices can exist in the protein backbone with a lifetime longer than around 10^{-6} s.

The organization of electron-transfer systems within mitochondrial membranes is known to play an important role in the compartmentalization of these processes and in exerting directional control over electron transfer. Apart from this "physical" influence, other components of mitochondrial membranes may become directly involved in the mechanisms of electron transfer between cytochrome proteins and complexes. For instance, cardiolipin, an anionic diphosphoglyceride localized in the inner mitochondrial membrane, is known to be required for optimal activity of the cytochrome *c* oxidase enzyme (Robinson et al., 1980; Marsh & Powell, 1988). The

† Work supported by The Science and Engineering Research Council under Grants GR/F/54006 and GR/E/56683 and under Grant GR/E/69188 (to A.W.).
* To whom correspondence should be addressed.

0006-2960/91/0430-3871$02.50/0